Evaluation of heavy metal migration at the Portsmouth Naval Shipyard with geochemical modeling

Andrew Reeve

December 31, 1997

1 Introduction

The Portsmouth Naval Shipyard (Kittery, Maine) currently maintains and repairs submarines. This facility has operated since 1800 and the first submarine was built in 1917 [2]. Waste disposal activities at the Portsmouth Naval Shipyard (PNS) associated with its operation represent a potential threat to ground-water and surface-water quality. Brown and Root Environmental was retained by the United States Navy to assess continuing transport of contaminants from the PNS to off-shore receptors. As part of their assessment, Brown and Root Environmental developed an analytical model to evaluate the the transport of contaminants by groundwater [2]. This modeling used Darcy calculations incorporating retardation and dilution by natural groundwater to calculate contaminant fluxes through the groundwater. In an effort to further evaluate the migration of heavy metals, computer simulations have been completed using a chemical equilibrium program [6].

2 General groundwater chemistry

The trends observed by plotting major ion chemistry data on a Piper plot [4] (figure 1) indicates that fresh-water and sea-water mixing is a dominant control on the general geochemistry of groundwater. Data that fall below the general mixing line (figure 1) suggest that either Na^+ is being exchanged for Ca^{2+} or carbonate minerals are being dissolved [1]. The exchange of Na^+ for Ca^{2+} typically occurs when an aquifer undergoes freshening and might be related to the creation or enhancement of a fresh-water lens in areas where fill was placed on marine sediments.

Box and whisker diagrams (figure 2) show the concentration range of heavy metals in groundwater samples collected at the PNS. Concentrations of metals in filtered and unfiltered samples are similar when samples are collected using low flow sampling techniques.

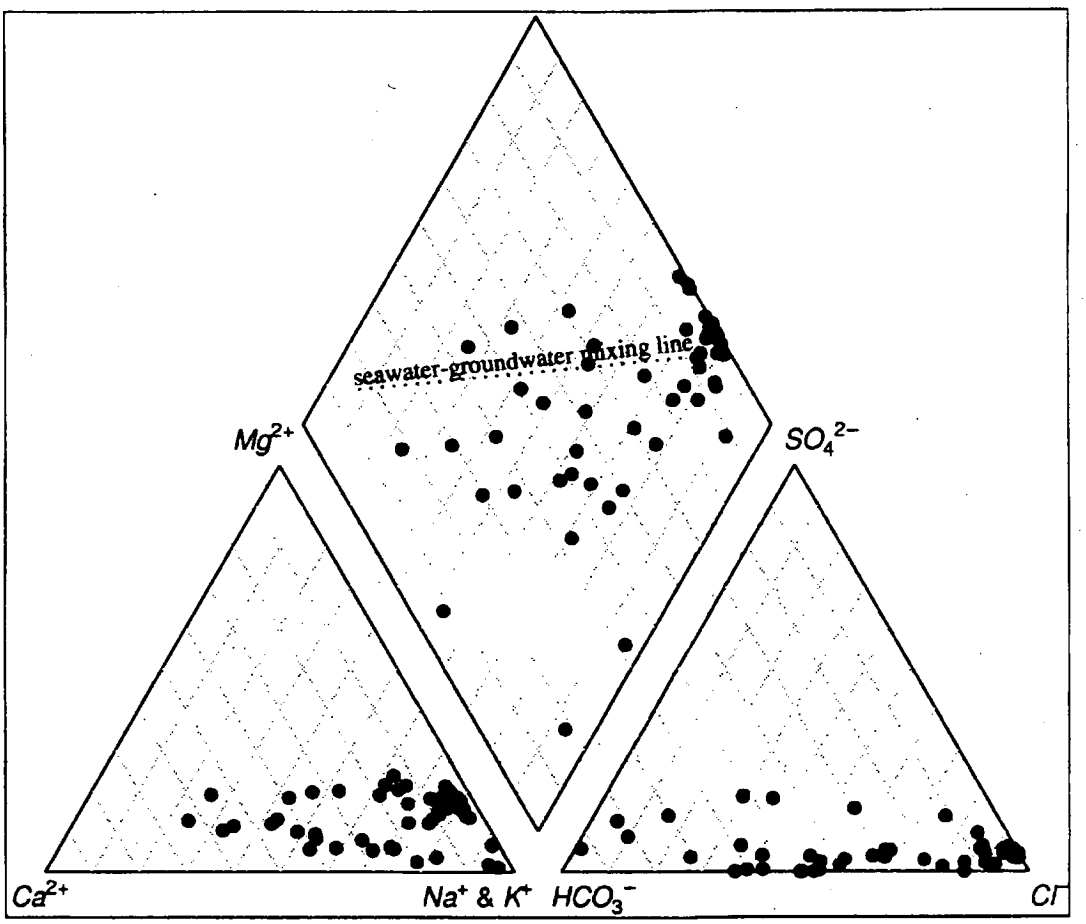

Figure 1: Piper plot displaying major ion chemistry of groundwater at the Portsmouth Naval Shipyard. The relative percentages of cations and anions (as equivalents per liter) in groundwater is plotted in the trilinear diagrams and then projected into the diamond shaped region. Concentrations range from 0% to 100% along the sides of each triangle.

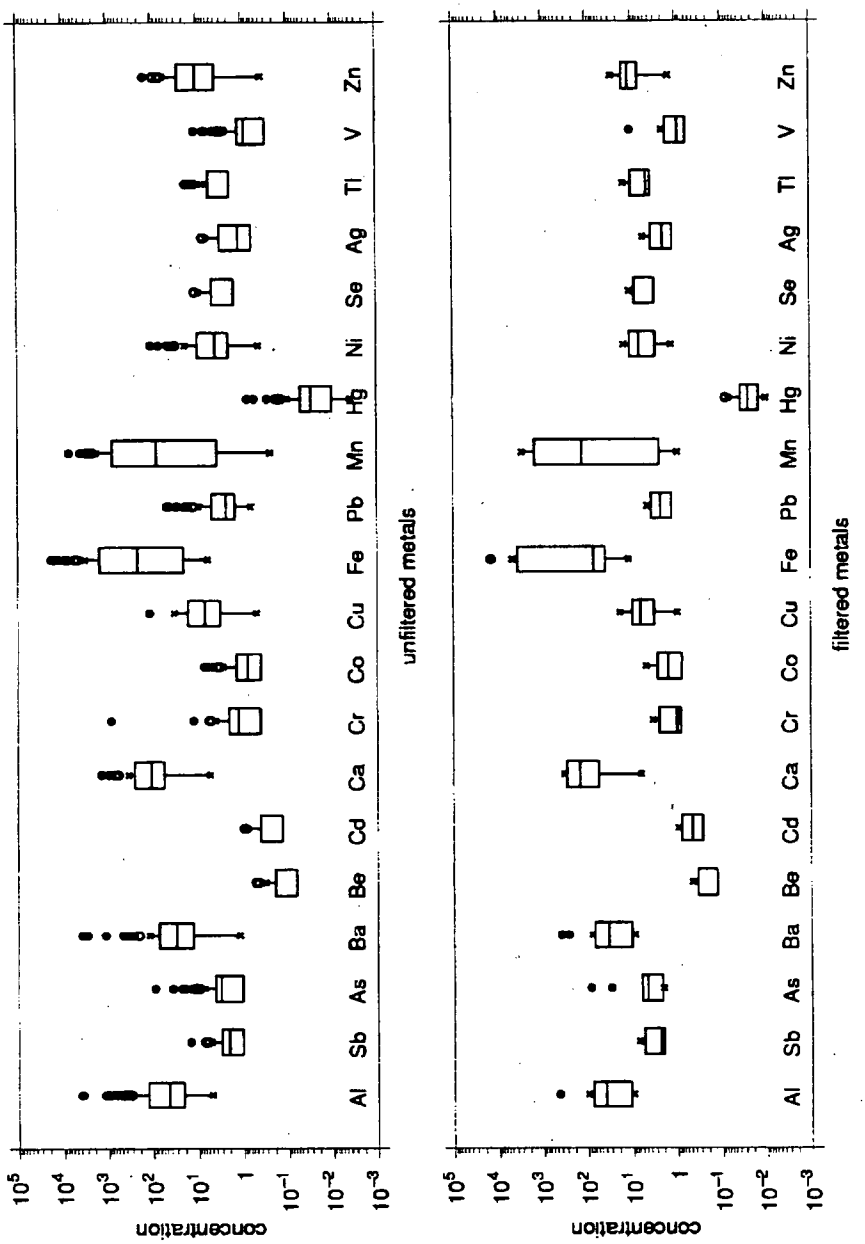

Figure 2: Box and whisker plots [8] of metal concentrations in the groundwater of the Portsmouth Naval Shipyard. All concentrations are in units of $\mu g \cdot \ell^{-1}$ except Ca, which is in units of $mg \cdot \ell^{-1}$. Boxes are bounded by the first quartile, median (second quartile), and third quartile. Whiskers extend to the nearest data point within a distance of 1.5 times the inter-quartile range. Circles are single data points located at a distance greater than 1.5 times the interquartile range. Data is for filtered and unfiltered samples collected using low flow sampling techniques

3 Methodology

3.1 Literature Search

The Dialog Database system at the University of Maine was utilized to search for literature related to heavy metal transport in groundwater systems linked to sea water systems. While the system identified several hundred citations that matched the search criterion, most of the articles are not directly relevant to groundwater quality at the PNS. A disk with the results of the database search are included and several relevant articles identified by this search are cited in this report.

3.2 Geochemical Modeling

Geochemical modeling was completed with the computer program PHREEQC [6]. Eight metals (mercury, copper, lead, aluminum, iron, manganese, nickel, and silver) were selected for evaluation based on ranking by Brown and Root Environmental [2]. PHREEQC is an equilibrium model with one-dimensional mass transport capabilities. This computer program calculates the aqueous species concentrations in equilibrium with mineral phases, surface complexation and ion exchange sites, and gas phases. Many of the parameters required by the model have been estimated from data presented in the Phase 1 modeling report prepared by Brown and Root Environmental [2]. In some cases a large amount of uncertainty is associated with these estimates. Dilution from recharge was not considered in the computer simulations.

PHREEQC calculates the concentration of aqueous species by solving a series of simultaneous equations based on mole balance and charge balance equations. These equations are iteratively solved using the Newton-Raphson method [6].

Two modeling approaches were used to evaluating the groundwater geochemistry of heavy metals at the PNS: 1) the saturation index of various minerals related to heavy metals were calculated at different redox potentials and different mixtures of fresh groundwater and sea water, and 2) one-dimensional advective transport models were constructed that incorporated surface complexation, ion exchange, mineral equilibrium, and the addition of salts associated with sea water.

Saturation indices were calculated in the first modeling approach for the end members, fresh and saline groundwater, and mixtures containing 20%, 40%, 60%, and 80% fresh groundwater. The oxidation-reduction potential was varied in these simulations by incrementally changing the partial pressure of O_2 from $10^{-52.7}$ to $10^{-68.7}$. Surface processes and organic compounds were not included in this series of simulations.

The second modeling approach required data to characterize cation exchange capacity, surface complexation, the specification phases that could be added and removed (Appendix 1), the concentration of solutes that entered the model, and the initial concentration of solute in each cell within the model (table 1).

Cation exchange capacity was calculated from the relationship [1]:

$$CEC = 0.7 \cdot (\%Clay) + 3.5 \cdot (\%Carbon)$$

	End Members (ppm)		Transport (ppm)	
Species	Fresh Water	Salt Water	Input Solution	Initial Solution
pH	6.9	7.7	6.9	6.9
Al	0.998	0.998	1.998	.998
As	0.088	0.088	1.088	0.0
Ba	3.78	3.78	3.78	3.78
Ca	45.8	352.	45.8	45.8
Cu	0.118	0.118	1.118	$5 \cdot 10^{-6}$
Ag	0.007	0.007	1.007	$1 \cdot 10^{-6}$
Mg	5.52	1070.	5.52	5.52
Na	17.9	8600	17.9	17.9
Pb	0.049	0.049	1.049	$3 \cdot 10^{-6}$
K	3.76	367	3.76	3.76
Fe	16.7	16.7	16.7	16.7
Mn	4.04	4.04	4.04	4.04
Hg	0.00078	0.00078	1.0078	$1 \cdot 10^{-6}$
Cl	5.7	16000.	15.7	15.7
S	11.67	600.25	11.67	11.67
N	6.2	0.22	6.2	6.2
Alkalinity	240	240	331.5	331.5
Zn	0.0899	0.0899	1.0899	0.0
Ni	0.106	0.106	1.106	$1 \cdot 10^{-6}$

Table 1: Concentrations (ppm) of chemicals used in simulations. Columns Labeled "End members" indicate concentrations in solutions used as end members in simulation approach #1. Columns labeled "Transport" indicate concentrations in solution that continuously enters the one-dimensional transport model and initial concentrations entered in all model cells before transport calculations began (approach #2). The organic compounds Acetate (0.1 ppm), Phthatate (0.1 ppm), and Tartrate (0.1 ppm) were included in transport solutions. Note that solutions used in approach #2 were equilibrated with mineral phases, lowering initial and inflow concentrations. Alkalinity is based on $Ca_{.5}(CO_3)_{0.5}$ in mixing simulations and HCO_3^- in transport simulations

Parameter	run 1	run 2	run 3	run 4	run 5	run 6
sea salt added	21-30	1-10	21-30	1-10	1-10	1-10
initial pe	0	0	0	0	4.7	-4
P_{O2}	10^{-50}	10^{-50}	10^{-60}	10^{-65}	10^{-40}	$10^{-71.5}$
surface complexation	0.0021	0.0021	0.00021	0.0021	0.0021	0.0021

Table 2: Primary differences in simulations. Sea salts were added to cells 21 to 30 and 1 to 10. Initial pe shown was adjusted to the specified P_{O2} while in equilibrium with various mineral phases. Surface complexation sites ($\frac{mol}{l}$) was lowered in run 3 to evaluate the importance of this variable on the migration of lead. Cation exchange sites were fixed at 0.6 $\frac{mol}{l}$ in all simulations.

Carbon concentration was taken from table A-1 from Brown and Root's Phase 1 Modeling Report and a clay content of 10% was assumed, resulting in 12.25 $\frac{meq}{100g}$ or 6.1 moles of exchanger per liter of water (Appendix 2).

Default values for equilibrium constants present in PHREEQC for reactions involving surface complexation sites were used in simulations and are based on the assumption that hydrous ferric oxides are primarily responsible for surface complexation in groundwater environments. Surface complexation sites were characterized with the weak binding site parameter (Hfo_w) available in PHREEQC. 1.05 moles of of iron are present in the sediment associated with each liter of water (Appendix 2) and 1 % of this iron was assumed to be associated with hydrous ferric oxides.

Salts were added to selected cells at a rate equivalent to mixing a cell with 1% sea water. This was done in 10 cells for a total salt addition equivalent to mixing groundwater with 10% seawater.

Mass transport in these simulations is purely advective and is done by moving the dissolved constituents from one reaction cell to the next in a conveyor belt fashion. All models were constructed with 30 reaction cells and were run for 100 time steps. The physical meaning of these parameters is dependent on the conceptualization of the model and the groundwater seepage velocity. If it is assumed that the model is about 600 feet long (approximate distance from waste sites to ocean) , then each cell is 20 feet long. The groundwater seepage velocity is about 2. $\frac{ft}{day}$ in the overburden at the PNS [2] resulting in a time step size of 10 days.

Parameters were varied in six simulations to characterize the importance of different geochemical processes (table 2).

4 Results and Discussion

Geochemical calculations suggest that redox potential is an important parameter for lead, copper, mercury, zinc, manganese, silver and iron solubility (figures 3-6). Redox potential was not an important factor for aluminum and nickel solubility (figures 3 and 4). Metals

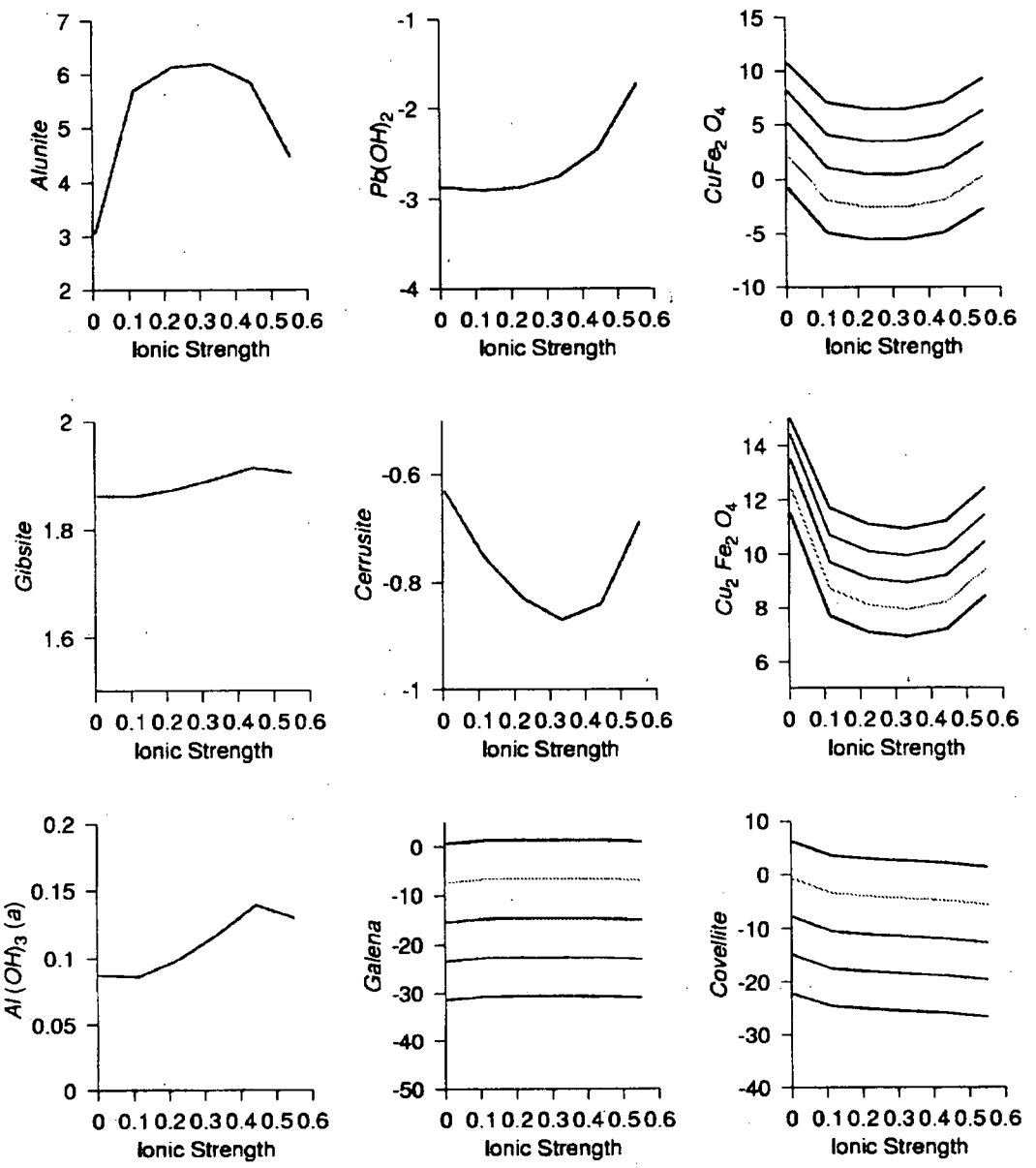

Figure 3: Calculated saturation index ($SI = \frac{ion\ activity\ product}{K_eq}$) verses ionic strength. The ionic strength is an indication of the proportions of saline and fresh groundwater that are mixed together to create the solution. Different curves in the graphs indicate saturation indices at different redox conditions: red line represents a $P_{O_2} = 10^{-52.72}\ atm$ ($pe \approx 2$), blue line represents a $P_{O_2} = 10^{-68.72}\ atm$ ($pe \approx -2$), lines between these extremes represent simulations set at pe's of approximately 1, 0, and -1). Note that pH increases with ionic strength on this diagram. (Alunite = $KAL_3(SO_4)_2(OH)_6$, Gibsite = $Al(OH)_3(c)$, Cerrusite = $PbCO_3$, Covellite = CuS)

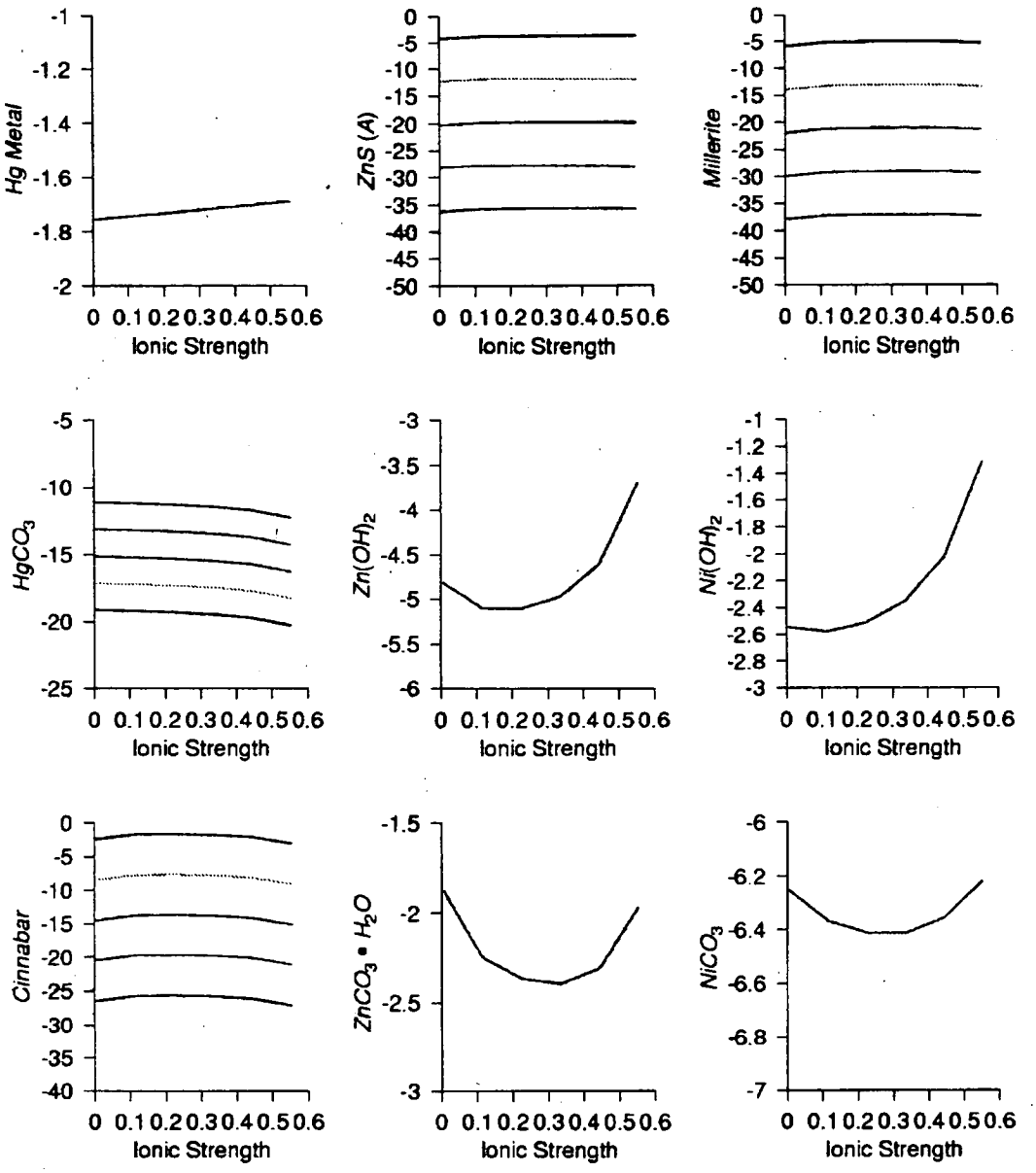

Figure 4: Calculated saturation index ($SI = \frac{ion\ activity\ product}{K_{eq}}$) verses ionic strength. The ionic strength is an indication of the proportions of saline and fresh groundwater that are mixed together to create the solution. Different curves in the graphs indicate saturation indices at different redox conditions: red line represents a $P_{O_2} = 10^{-52.72}\ atm$ ($pe \approx 2$), blue line represents a $P_{O_2} = 10^{-68.72}\ atm$ ($pe \approx -2$), lines between these extremes represent simulations set at pe's of approximately 1, 0, and -1). Note that pH increases with ionic strength on this diagram. (Cinnabar = HgS, Millerite = NiS)

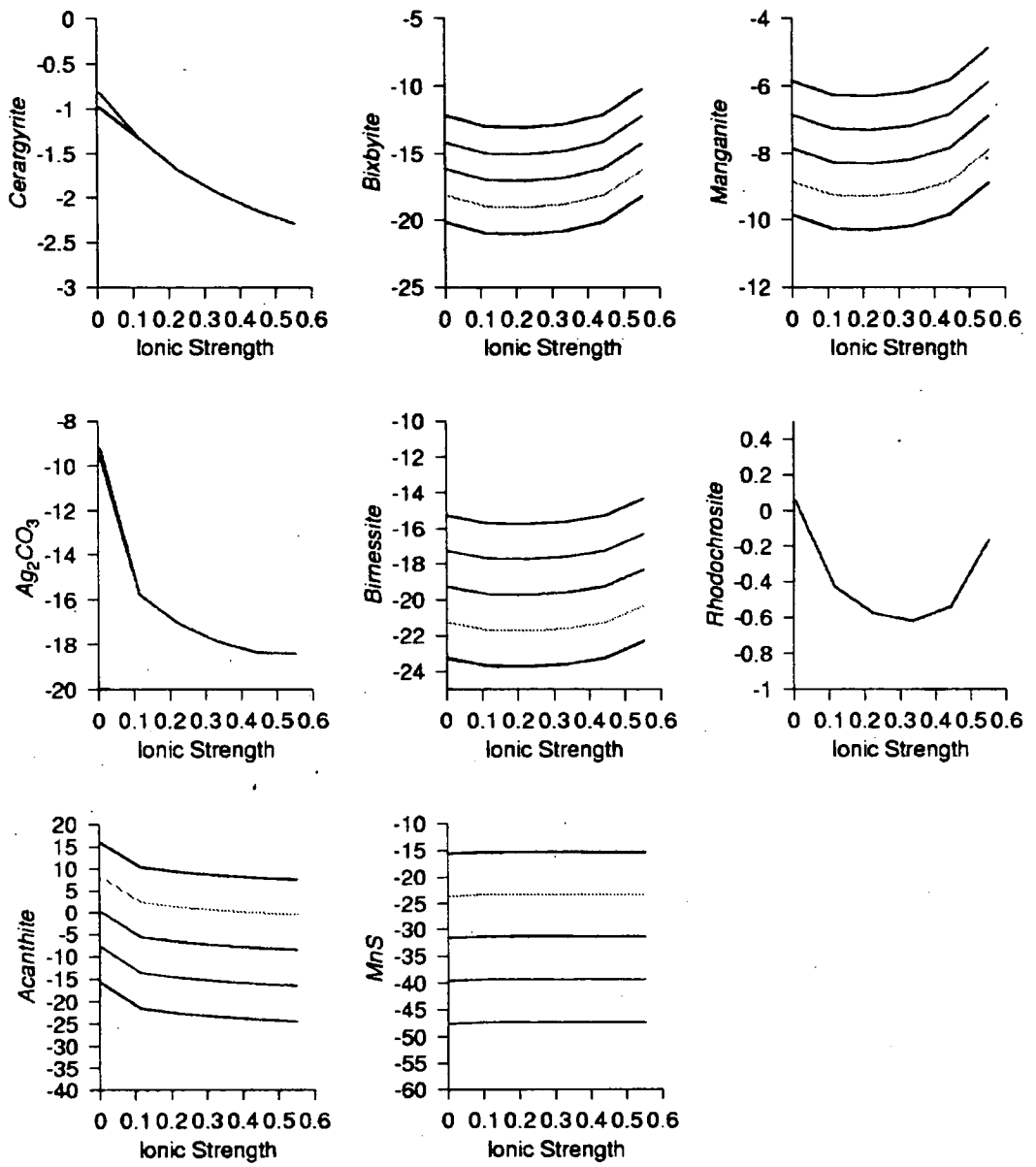

Figure 5: Calculated saturation index ($SI = \frac{ionactivityproduct}{K_{eq}}$) verses ionic strength. The ionic strength is an indication of the proportions of saline and fresh groundwater that are mixed together to create the solution. Different curves in the graphs indicate saturation indices at different redox conditions: red line represents a $P_{O_2} = 10^{-}52.72\ atm$ ($pe \approx 2$), blue line represents a $P_{O_2} = 10^{-}68.72\ atm$ ($pe \approx -2$), lines between these extremes represent simulations set at pe's of approximately 1, 0, and -1). Note that pH increases with ionic strength on this diagram. (Cerrargyrite = $AgCl$, Bixbyite = Mn_2O_3, Rhodochrosite = $MnCO_3$, Manganite = $MnOOH$, Birnessite = MnO_2, Acanthite = Ag_2S)

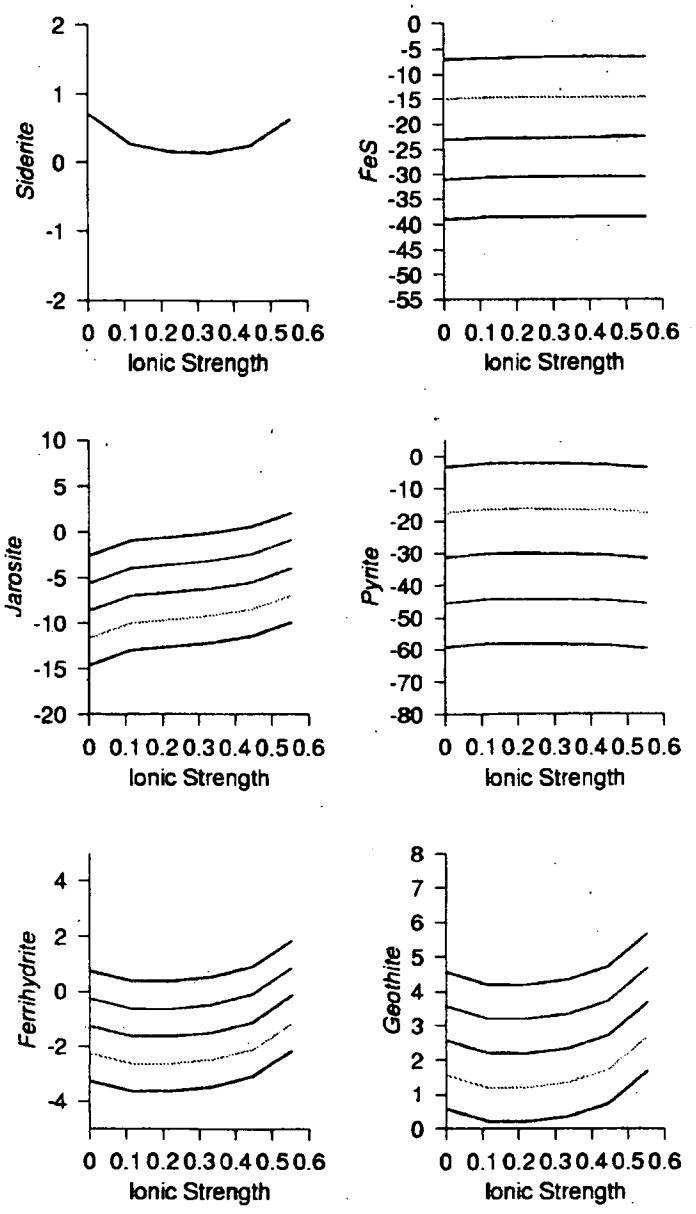

Figure 6: Calculated saturation index ($SI = \frac{ionactivityproduct}{K_{eq}}$) verses ionic strength. The ionic strength is an indication of the proportions of saline and fresh groundwater that are mixed together to create the solution. Different curves in the graphs indicate saturation indices at different redox conditions: red line represents a $P_{O_2} = 10^{-}52.72\ atm$ ($pe \approx 2$), blue line represents a $P_{O_2} = 10^{-}68.72\ atm$ ($pe \approx -2$), lines between these extremes represent simulations set at pe's of approximately 1, 0, and -1). Note that pH increases with ionic strength on this diagram. (Ferrihydrite = $Fe(OH)_3$, Jarosite = $KFe_3(SO_4)_2(OH)_6$), Siderite = $FeCO_3$, Pyrite = FeS

that did not have variable valance states were influenced by redox potentials through the formation of sulfide mineral phases. Heavy metal concentrations measured in groundwater samples collected at the PNS indicate that they are not controlled by equilibrium with mineral with the exception of aluminum, iron, and manganese. Aluminum is near equilibrium conditions with the amorphose $Al(OH)_3$ and supersaturated with respect to gibsite (figure 3), suggesting that these phase regulates aluminum solubility in samples with high concentrations of aluminum. Saturation index calculations for Rhodochrosite indicate that this phase is in equilibrium with groundwater at low ionic strength (fresh groundwater) conditions suggesting that this phase may limit manganese concentration (figure 5). Similarly, Siderite, Geothite, and Ferrihydrite may limit the concentration of iron in groundwater at the PNS (figure 6).

Transport models indicate that surface complexation dramatically lower the total aqueous concentration of lead. However, uncharged heavy metal species, such as Hg^0 and $PbCO_3^0$ do not participate in surface reactions and will not be retarded by surface processes. The strong affinity of lead for surface complexation sites prevented other metals from being sorbed by surface complexation sites. The importance of surface complexation on lead concentration is shown in all transport simulations by the steady increase in lead concentrations over time, reflecting the slow saturation of surface complexation sites (figures 7-12). The lead concentration rapidly decreases between cell 2 and 3 after 100 time steps, indicating that surface sites in cell 2 are becoming saturated but are still undersaturated in cell 3 (figure 13). The impact of oxidation-reduction potential on metal concentrations is also present in transport simulations. Dissolved mercury occurs as primarily Hg^0 in simulations with pe of about -2 and 5 (figures 7 - 11), and is very mobile in this form maintaining concentrations of about $2.5 \cdot 10^{-7} \frac{mol}{Kg}$ (50 ppb). This concentration reflects equilibrium conditions between Hg^0 and mercury metal. Under more reducing conditions ($pe < -2$) mercury precipitates in sulfide phases and concentrations drop to less than 1 ppb (figure 12). The precipitation of sulfides under reducing conditions also results in the removal of iron and lead from solution (figure 12). Copper concentrations were very low in all simulations and are controlled by the precipitation of Copper Ferrite phases (not shown in figures). Iron is mobile under reducing conditions ($pe \approx -2$, 12, 10) but is relatively insoluble under more oxidizing conditions.

Adding sea salts to cells 1 through 10 did not result in significant changes in the concentrations of metals in solution (figures 7-8). The addition of sea salts did lower pH through the mobilization of $H+$ by cation exchange and this resulted in a short term increase in Mn and Fe concentrations.

Organic substances included in the simulations did not significantly increase heavy metal concentrations. Other ligands, such as CO_3^{2-} and S^{2-} were more important complexing agents for the heavy metals. Organic ligands formed complexes with Ca^{2+} due to its high concentrations, limiting its availability to heavy metals. Similar results were observed in laboratory experiments [3]. This may change with the consideration of other organic compound or increase in the concentration of organic compounds.

Maximum metal concentrations calculated in numerical simulations differ from metal concentrations measured in groundwater (table 3). I attribute this to the following fac-

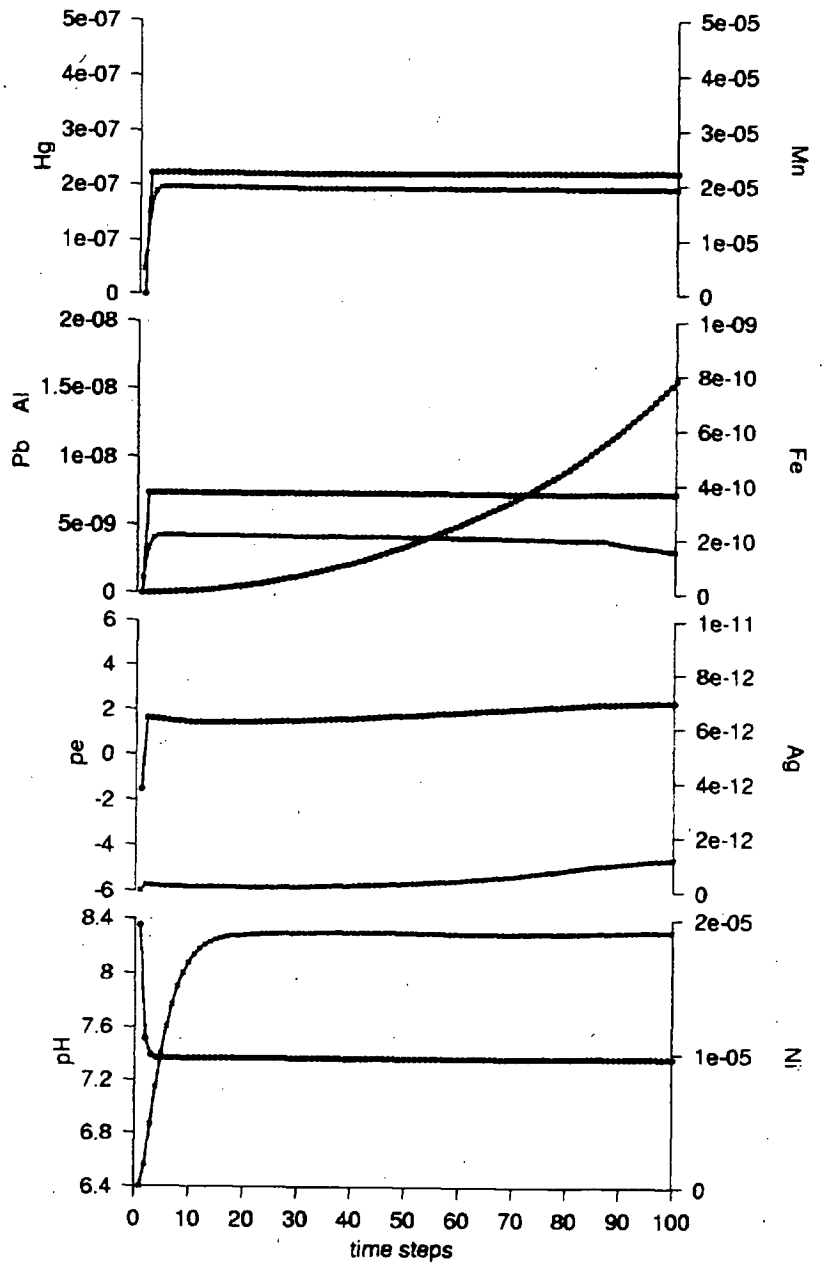

Figure 7: Concentration ($\frac{mol}{l}$) of heavy metals in cell 2 of simulation (run 1) over time. Each time step represents the amount of time required to flush a cell by advective transport.

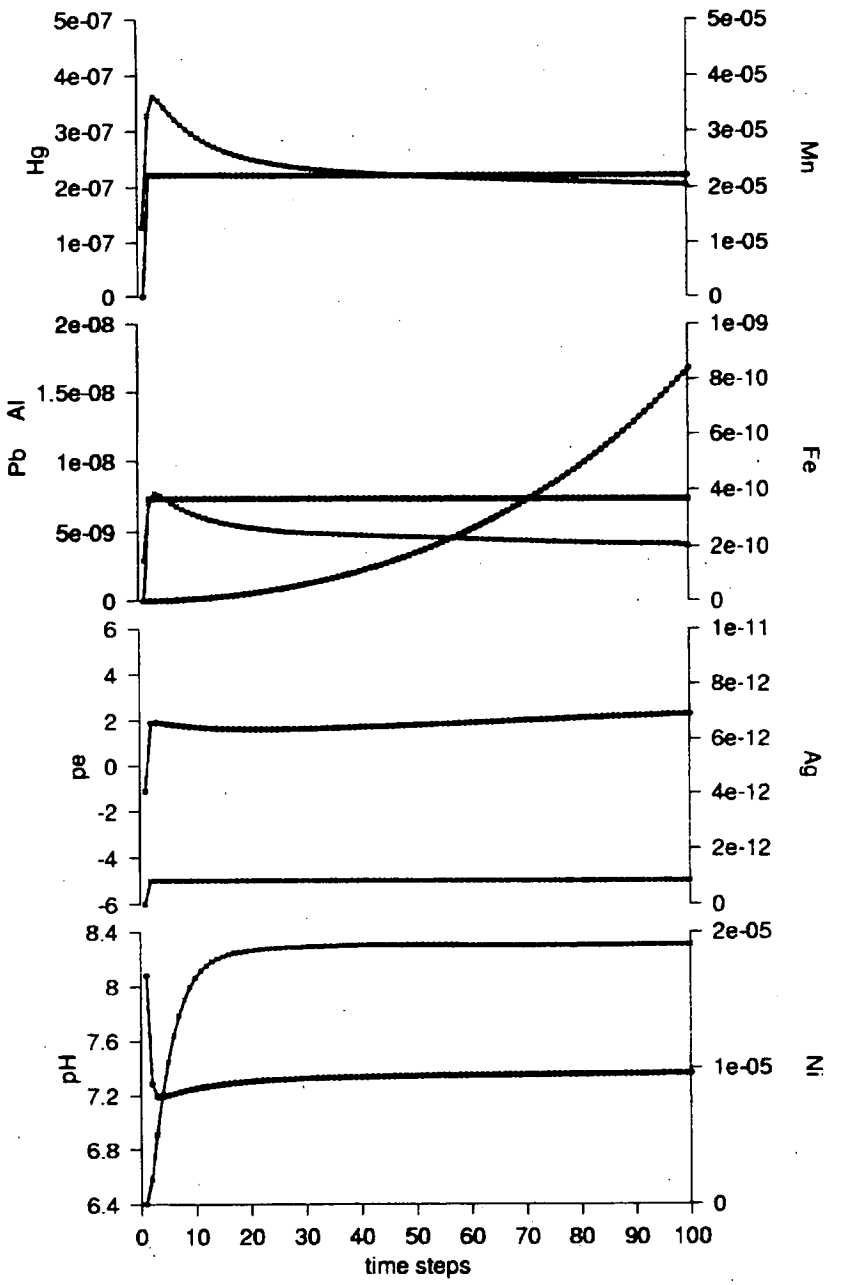

Figure 8: Concentration ($\frac{mol}{l}$) of heavy metals in cell 2 of simulation (run 2) over time. Each time step represents the amount of time required to flush a cell by advective transport.

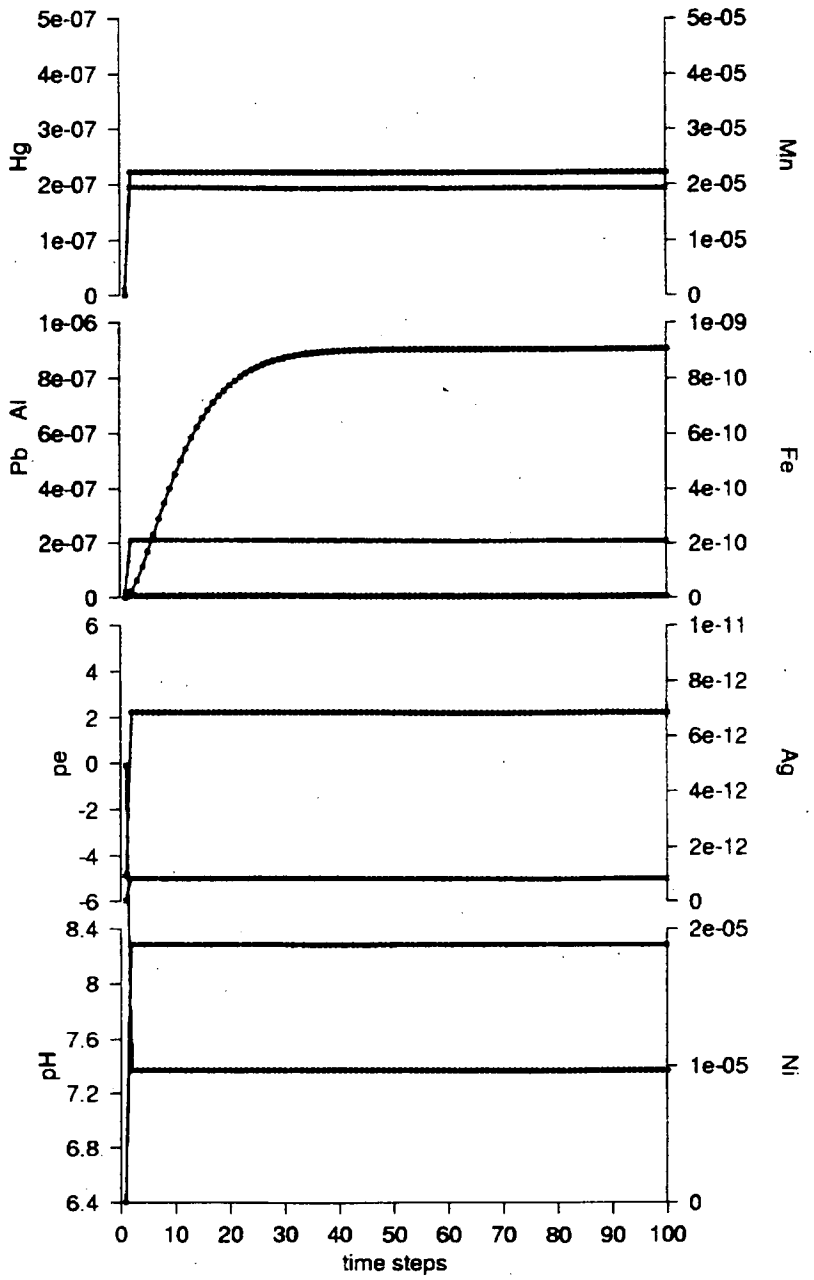

Figure 9: Concentration ($\frac{mol}{l}$) of heavy metals in cell 2 of simulation (run 3) over time. Each time step represents the amount of time required to flush a cell by advective transport.

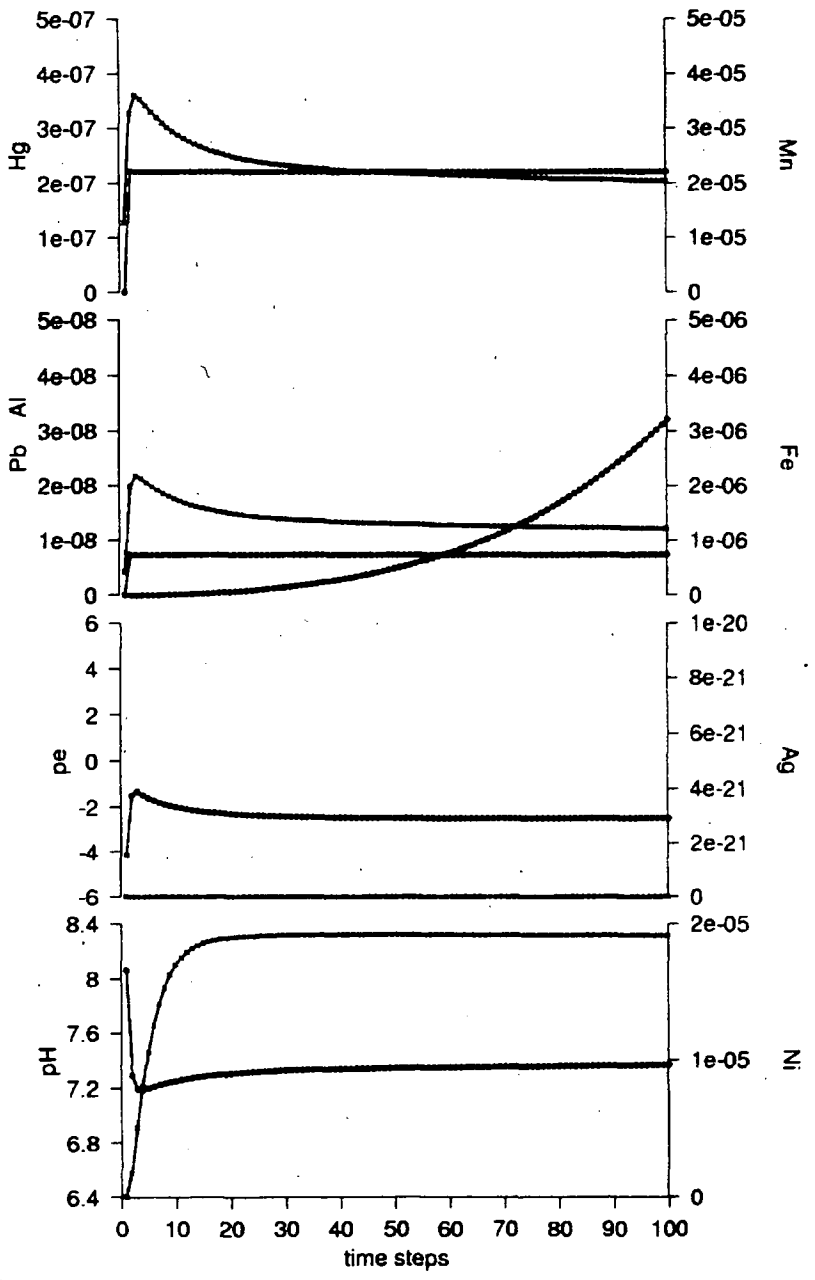

Figure 10: Concentration ($\frac{mol}{l}$) of heavy metals in cell 2 of simulation (run 4) over time. Each time step represents the amount of time required to flush a cell by advective transport.

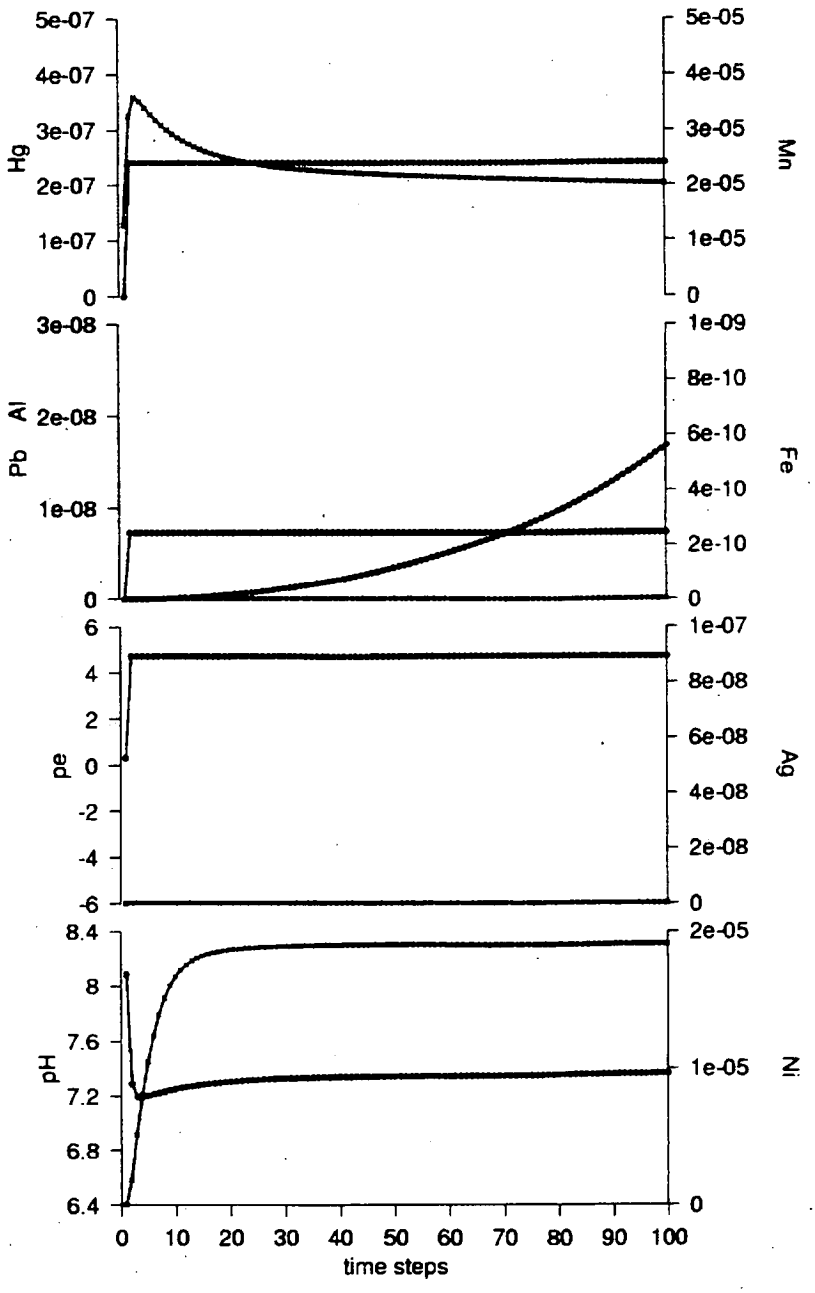

Figure 11: Concentration ($\frac{mol}{l}$) of heavy metals in cell 2 of simulation (run 5) over time. Each time step represents the amount of time required to flush a cell by advective transport.

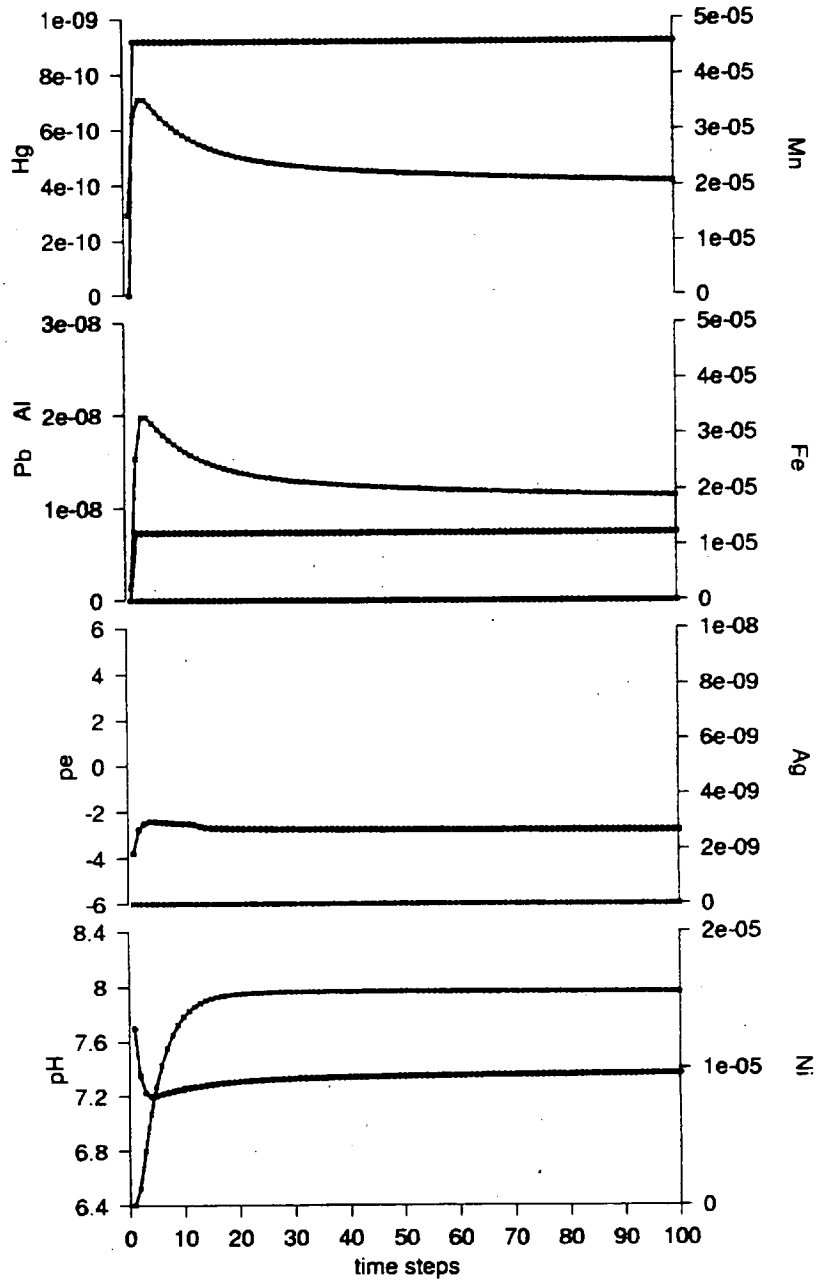

Figure 12: Concentration ($\frac{mol}{l}$) of heavy metals in cell 2 of simulation (run 6) over time. Each time step represents the amount of time required to flush a cell by advective transport.

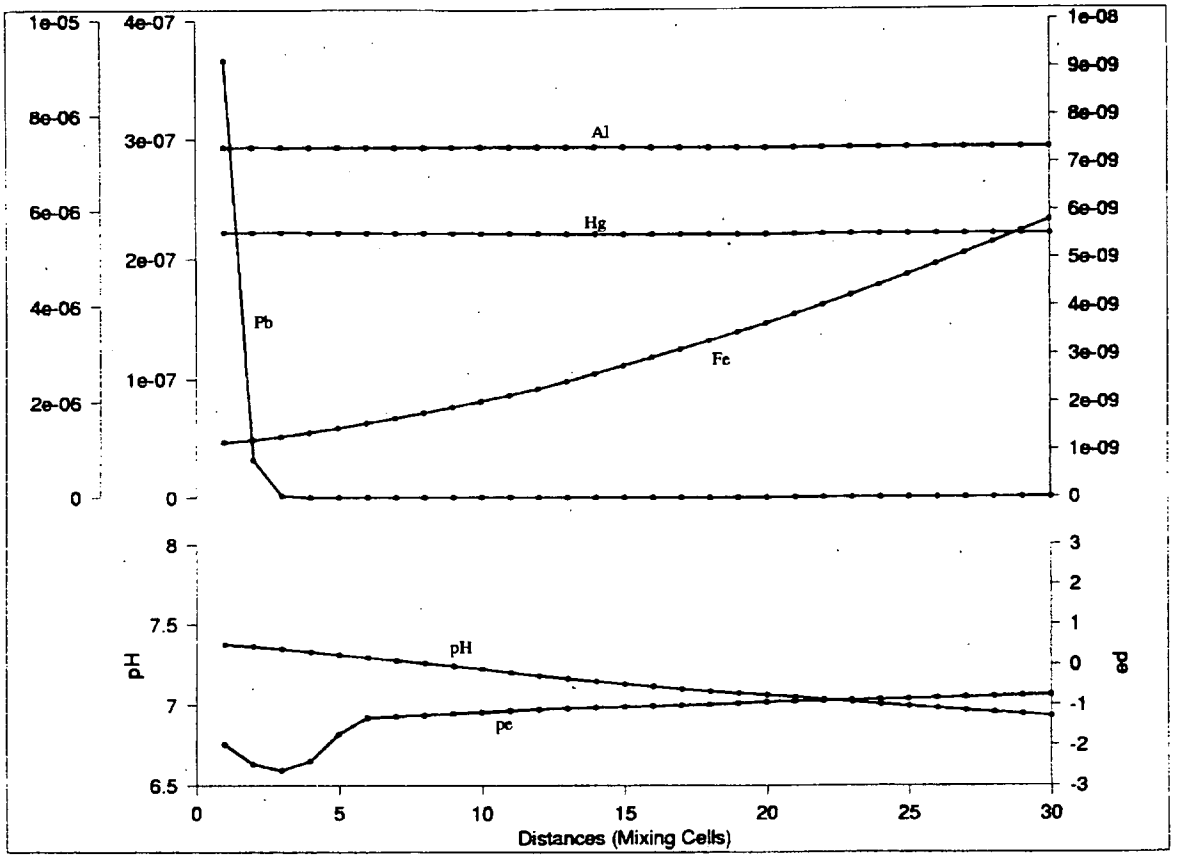

Figure 13: Concentration ($\frac{mol}{l}$) of heavy metals after 100 time steps in computer simulation. Parameters in this simulation are the same as used for run 4 (figure 10). simulation over time. Each time step represents the amount of time required to flush a cell by advective transport.

Metal	Simulated $mol \cdot l^{-1}$	Simulated $\mu g \cdot l^{-1}$ (ppb)	Measured $\mu g \cdot l^{-1}$ (ppb)	C(source)
Mercury (Hg)	$2.2 \cdot 10^{-7}$	44	0.78	19.9
Lead (Pb)	$9 \cdot 10^{-7}$	186	49	3740
Aluminum (Al)	$8 \cdot 10^{-8}$	2	3940	97200
Manganese (Mn)	$2 \cdot 10^{-5}$	1100	7220	3830
Iron (Fe)	$2 \cdot 10^{-5}$	1120	18400	1340000
Silver (Ag)	$1 \cdot 10^{-12}$	$1 \cdot 10^{-4}$	6.4	45.7
Nickel (Ni)	$1 \cdot 10^{-5}$	590	106	3850
Copper (Cu)	$3 \cdot 10^{-14}$	$2 \cdot 10^{-6}$	33	10100

Table 3: Comparison of simulated and measured metal concentrations in the groundwater at the PNS. C(source) is the source concentration at OU3 (Back Channel) used in simulations conducted by Brown and Root Environmental [2]

tors: 1) redox potentials is very difficult to measure and the range of values used in simulations (based on unpublished data collected by Brown and Root) may not be representative of subsurface conditions, 2) dilution was not considered in these models and is an important factor at the site, 3) slow kinetics of chemical reactions may prevent equilibrium conditions from being reached, 4) colloid may be important in transport and have not been considered in the simulations, and 5) variation in geochemical conditions along a flow path have not been considered.

Despite these weaknesses the numerical simulations provide insight on geochemical processes that will be important in regulating the heavy metal concentrations in groundwater at the PNS. The concentrations of Hg, Pb and Ni were higher in simulations than were measured in groundwater. Surface complexation is important in regulating the concentrations of Pb and Ni, and the low concentration of surface complexation sites incorporated into simulations may partially explain these results. The high simulated concentrations of Hg are related to the occurrence of Hg^0 in solution. If more oxidizing conditions are present at the waste source, as would be expected, Hg^{2+} would be the dominant species and this would react with surface complexation sites and form solid phases with low solubility [7], lowering its concentration. Concentrations of Fe, Mn, Al, Ag, and Cu are all lower in the simulations than in groundwater. These may result from the inclusion of solid particulates, colloids or organic complexes in groundwater samples, elevating the measured concentration of heavy metals. This is supported by the high turbidity measured in water samples with the highest concentrations of Fe, Mn, and Al.

5 Conclusion

Geochemical modeling indicates that the addition of salts from mixing of sea water with the fresh groundwater lens will not have a large impact due to changes in ionic strength of solutions. Salts supplied by sea water will interact with cation exchange and surface complexation sites, lowering the sediments ability to retard the migration of metals. Sea water influx will be an important source of sulfide that forms solid phases with many of the heavy metals of concern under reducing conditions, limiting the concentration of heavy metal. Under appropriate oxidation-reduction potential, precipitation of mineral phases removed heavy metals from the solution and limited their solubility. Surface complexation was extremely important in retarding lead migration but was not important in retarding the migration of other heavy metals. This result may be partially due to the conservative estimate of surface complexation sites in sediments at the PNS. Estimates of surface complexation sites used in this model are an order of magnitude smaller than published values [5, 9].

The analytical modeling completed by Brown and Root Environmental appears to be based on steady state simulations. Under this assumption retardation factors will not be important in calculating flux rates of metals through the groundwater as retardation only slows the migration of waste for a limited amount of time. Accurate estimation of distribution coefficients is not required under steady state conditions, except for the calculation of source concentrations.

Source concentrations far exceeded equilibrium concentrations calculated in computer simulations, with the exception of Mn 3. The metal concentrations in source areas was calculated based on concentrations of metals in sediments obtained from the waste sites (C_s) and retardation factors (K_d):

$$C_{source} = \frac{C_s}{K_d}$$

This approach results in elevated concentrations because metal concentrations measured in sediments may be present as solid phases and not sorbed to surface. Chemical equilibrium calculations based on most conservative assumptions might provide an alternative tool for estimating source area concentrations that are more realistic if waste products are known.

References

[1] C. Appelo and D. Postma. *Geochemistry, groundwater and pollution.* A. A. Balkema, Rotterdam, 1994. 536 p.

[2] Brown and Root Environmental. On-shore/off-shore contaminant fate and transport modeling phase I report for Portsmoth Naval Shipyard, Kittery, Maine. Technical report, 1997.

[3] Y. Cao, M. Conklin, and E Betterton. Competative compexation of trace metals with dissolved humic acids. *Environmental Health Perspectives*, 103(suppl 1):29–32, 1995.

[4] A. Freeze and J. Cherry. *Groundwater*. Prentice-Hall, Englewood Cliffs, NJ, 1979.

[5] C. Fuller, J. Davis, J. Coston, and E. Dixon. Characterization of metal adsorbtion variability in a sand and gravel aquifer, Cape Cod, Massachusetts, U.S.A. *Journal of Contaminant Hydrology*, 22:165–187, 1996.

[6] D. Parkhurst. User's guide to PHREEQC - a computer program for speciation, reaction path, advective-transport, and inverse geochemical calculations. Water-resources investigation report 95-4227, U.S. Geological Survey, 1995.

[7] E. Steinnes. Mercury. In B. Alloway, editor, *Heavy metals in soil*, pages 245–259. Blackie Academic, 1995.

[8] J. Tukey. *Exporatory Data Analysis*. Addison-Wesley, 1977.

[9] F. Wang, J.Chen, and W. Forsling. Modeling sorbtion of trace metals on natural sediments by surface complexation model. *Environmental Science and Technology*, pages 448–453, 1997.

6 Appendix 1

Input file for a transport model showing parameters used in a simulation "run 1". Similar parameters were used in other simulations.

```
TITLE transport of metals at the Portsmouth Naval Shipyard
Solution 0
    temp 10.
    units ppm
    pH  6.9
    pe  0.0
    Al  1.998
    As  1.0878
    Ba  3.78
    Ca  45.8
    Ni  1.106
    Cu  1.118
    Ag  1.0071
    Mg  5.52
    Na 17.9
    Pb  1.0492
    K   3.76
    Fe  16.7
    Mn  4.04
    Hg  1.0078
    Cl  15.7 charge
    S    11.67
    N    6.2
    C  331.535 as HCO3
    Zn  1.0899
    Acetate 0.1
#    Nta        0.1
    Phthalate   0.1
    Tartrate    0.1
EQUILIBRIUM_PHASES 0
    Calcite     0.1     10.
    CO2(g)      -2.     10.
    O2(g)       -50     10.
    Quartz      0.      10.
#Mercury
    Cinnabar    0.  0.
    HgMetal     0.  0.
    HgCO3       0.  0.
    Metacinnabar    0.  0.
#Aluminum
    Al(OH)3(a)  0.  0.
    Al2O3       0.  0.
    Alunite     0.  0.
    Boehmite    0.  0.
    Diaspore    0.  0.
    Gibbsite(C) 0.  0.
#Copper
#    Chalcocite  0.  0.
    Cu(OH)2     0.  0.
    CuCO3       0.  0.
    CuMetal     0.  0.
    CupricFerrite   0.  0.
    CuprousFerrite  0.  0.
#Lead
    Cerrusite   0.  0.
    Galena      0.  0.
    Pb(OH)2(C)  0.  0.
    PbMetal     0.  0.
#Nickle
    Millerite   0.  0.
    Ni(OH)2     0.  0.
    NiCO3       0.  0.
#Iron
    Ferrihydrite    0.  0.
    FeS(ppt)        0.  0.
    Goethite        0.  0.
    Jarosite-K      0.  0.
#    Pyrite         0.  0.
    Siderite        0.  0.
#Manganese
#    MnS(Green)     0.  0.
    Manganite       0.  0.
```

```
    Nsutite          0.  0.
    Pyrocroite       0.  0.
    Pyrolusite       0.  0.
    Rhodochrosite    0.  0.
#Silver
    Acanthite        0.  0.
    AgMetal          0.  0.
    Cerargyrite      0.  0.
#SURFACE 0
#    -equil solution 0
#    Hfo_w   0.068    600.      60.5
SAVE Solution 0
END

SOLUTION 99
    temp 10.
    units ppm
    pH  6.9
    pe  0.0
    Al  0.998
    Ca  45.8
    Mg  5.52
    Na 17.9
    K   3.76
    Fe  16.7
    Mn  4.04
    Cl  15.7 charge
    S    11.67
    N    6.2
    Ag  0.000001
    Pb  0.000003
    Cu  0.000005
    Hg  0.000001
    Ni  0.000001
    C  331.535 as HCO3
EQUILIBRIUM_PHASES 99
    Calcite      0.1      10.
    CO2(g)       -2.      10.
    O2(g)        -50.     10.
    Quartz       0.       10.
#Mercury
    Cinnabar     0.  0.
    HgMetal      0.  0.
    HgCO3        0.  0.
    Metacinnabar     0.  0.
#Aluminum
    Al(OH)3(a)   0.  0.
    Al2O3        0.  0.
    Alunite      0.  0.
    Boehmite     0.  0.
    Diaspore     0.  0.
    Gibbsite(C)  0.  0.
#Copper
#    Chalcocite  0.  0.
    Cu(OH)2      0.  0.
    CuCO3        0.  0.
    CuMetal      0.  0.
    CupricFerrite    0.  0.
    CuprousFerrite   0.  0.
#Lead
    Cerrusite    0.  0.
    Galena       0.  0.
    Pb(OH)2(C)   0.  0.
    PbMetal      0.  0.
#Nickle
    Millerite    0.  0.
    Ni(OH)2      0.  0.
    NiCO3        0.  0.
#Iron
    Ferrihydrite     0.  0.
    FeS(ppt)         0.  0.
    Goethite         0.  0.
```

```
    Jarosite-K       0.  0.
#    Pyrite          0.  0.
    Siderite         0.  0.
#Manganese
#    MnS(Green)      0.  0.
    Manganite        0.  0.
    Nsutite          0.  0.
    Pyrocroite       0.  0.
    Pyrolusite       0.  0.
    Rhodochrosite    0.  0.
#Silver
    Acanthite        0.  0.
    AgMetal          0.  0.
    Cerargyrite      0.  0.
SAVE Solution 99
END

SOLUTION 1-30
    USE Solution 99
EXCHANGE 1-30
    equil 99
    X   .6
SURFACE 1-30
    -equil 99
    Hfo_w   0.0021       300.    95.
REACTION 21-30
    NaCl     0.468
    KCl      0.01
    CaSO4    0.01
    MgSO4    0.018
    MgCl2    0.034
    MgCO3    0.0013
    .005 moles in 1 step
EQUILIBRIUM_PHASES 1-30
    Calcite      0.1      10.
#    CO2(g)      -2.      10.
#    O2(g)       -60.     10.
    Quartz       0.       10.
#Mercury
    Cinnabar     0.  0.
    HgMetal      0.  0.
    HgCO3        0.  0.
    Metacinnabar     0.  0.
#Aluminum
    Al(OH)3(a)   0.  0.
    Al2O3        0.  0.
    Alunite      0.  0.
    Boehmite     0.  0.
    Diaspore     0.  0.
    Gibbsite(C)  0.  0.
#Copper
#    Chalcocite  0.  0.
    Cu(OH)2      0.  0.
    CuCO3        0.  0.
    CuMetal      0.  0.
    CupricFerrite    0.  0.
    CuprousFerrite   0.  0.
#Lead
    Cerrusite    0.  0.
    Galena       0.  0.
    Pb(OH)2(C)   0.  0.
    PbMetal      0.  0.
#Nickle
    Millerite    0.  0.
    Ni(OH)2      0.  0.
    NiCO3        0.  0.
#Iron
    Ferrihydrite     0.  0.
    FeS(ppt)         0.  0.
    Goethite         0.  0.
    Jarosite-K       0.  0.
#    Pyrite          0.  0.
```

```
    Siderite        0.  0.
#Manganese
#    MnS(Green)     0.  0.
    Manganite       0.  0.
    Nsutite         0.  0.
    Pyrocroite      0.  0.
    Pyrolusite      0.  0.
    Rhodochrosite   0.  0.
#Silver
    Acanthite       0.  0.
    AgMetal         0.  0.
    Cerargyrite     0.  0.
TRANSPORT
    -cells 30
    -shifts 100
    -print 1
PRINT
    -reset  false
    -species    false
SELECTED_OUTPUT
    -file trnsp.std.tbl
    -totals Pb Hg As Ag Cu Ni Al Fe Mn
KNOBS
    -iterations 1000
    -diagonal_scale true
    -step_size 5
END
```

7 Appendix 2

Calculation of grams of sediment associated with 1 liter of solution

The parameters in the geochemical program PHREEQC require that they be cast in terms of liters of solution. Many parameters are typically expresses in terms of sediment mass requiring the conversion between liters of solution and mass of sediment.

$$\frac{grams\ sediment}{liter\ H_2O} = 1\ \ell\ H_2O \cdot \frac{1000\ cm^3\ H_2O\ and\ sed.}{0.3\ \ell\ H_2O} \cdot \frac{1.5\ g\ sed. + 0.3\ g\ H_2O}{1cm^3\ H_2O\ andsed.}$$

Porosity of the sediment = 0.3 dry bulk density of sediment is 1.5 $\frac{g}{cm^3}$

$$1\ \ell\ H_2O = 6000\ g\ sed.$$

Calculation of Surface Complexation Sites

Assume 1% Iron in soils.

$$\frac{6000\ g\ sed}{1\ \ell\ H_2O} \cdot \frac{1\ g\ Fe}{100\ g\ sed.} = \frac{60\ g\ Fe}{\ell\ H_2O}$$

$$\frac{60\ g\ Fe}{\ell\ H_2O} \cdot \frac{1\ mole\ Fe}{55.85\ g} = \frac{1.07\ moles\ Fe}{\ell\ H_2O}$$

Assuming 1% of iron is present as Hydrous Ferric Oxides (HFO) results in $\frac{.0107\ moles\ HFO}{\ell\ H_2O}$.
Assuming 0.2 moles of sites per mole of HFO yields $\frac{2.1 \cdot 10^{-3}\ sites}{\ell\ H_2O}$

Calculation of Cation Exchange Sites

The cation exchange capacity was calculated using [1]:

$$CEC(\frac{meq}{100\ g\ sed}) = 0.7 \cdot (\%Clay) + 3.5 \cdot (\%Carbon)$$

%clay was assumed to be 10% and %C was assigned a value of 1.5% based on table A-1 of the Phase 1 fate and transport modeling report prepared by Brown and Root Environmental [2].

$$CEC = 12.25\frac{meq}{100\ g}$$

Each liter of water comes in contact with 6000 g of sediment, therefore each liter of water is equilibrates with:

$$CEC\frac{meq}{\ell\ H_2O} = \frac{6000\ g}{\ell} \cdot \frac{12.25meq}{100\ g\ sed/} = 0612.5\frac{meq}{\ell}$$